


Genetic algorithm-*de novo*, molecular dynamics and MMGBSA based modelling of a novel Benz-pyrazole based anticancer ligand to functionally revert mutant P53 into wild type P53

Ashik Chhetri, Moloy Roy, Puja Mishra, Amit Kumar Halder, Souvik Basak, Aditi Gangopadhyay, Achintya Saha & Plaban Bhattacharya


To cite this article: Ashik Chhetri, Moloy Roy, Puja Mishra, Amit Kumar Halder, Souvik Basak, Aditi Gangopadhyay, Achintya Saha & Plaban Bhattacharya (2023) Genetic algorithm-*de novo*, molecular dynamics and MMGBSA based modelling of a novel Benz-pyrazole based anticancer ligand to functionally revert mutant P53 into wild type P53, Molecular Simulation, 49:7, 678-689, DOI: [10.1080/08927022.2023.2185079](https://doi.org/10.1080/08927022.2023.2185079)

To link to this article: <https://doi.org/10.1080/08927022.2023.2185079>

 View supplementary material 

 Published online: 09 Mar 2023.

 Submit your article to this journal 

 Article views: 166

 View related articles 

 View Crossmark data 

 Citing articles: 1 View citing articles 



Genetic algorithm-*de novo*, molecular dynamics and MMGBSA based modelling of a novel Benz-pyrazole based anticancer ligand to functionally revert mutant P53 into wild type P53

Ashik Chhetri^a, Moloy Roy^a, Puja Mishra^a, Amit Kumar Halder^a, Souvik Basak^a, Aditi Gangopadhyay^b, Achintya Saha^b and Plaban Bhattacharya^{b,c}

^aDr. B.C. Roy College of Pharmacy & Allied Health Sciences, Durgapur, India; ^bDepartment of Chemical Technology, University of Calcutta, Kolkata, India; ^cOrange Business, Vishwaroop IT Park, Navi Mumbai, India

ABSTRACT

Mutations in P53 cause a loop unfolding, resulting in loss of activity and finally leading to cancer. One strategically reported way to arrest such oncogenesis is the restoration of tertiary structure as well as the function of mutant P53. In this attempt, we have designed a benzo-pyrazole-based novel ligand starting from a carbazole compound (EYB or PK9324) reported earlier to reinstate such function in mutant P53 (Y220C mutant, PDB: 6GGD). Assuming PK9324 as the template scaffold, *de novo* technique (Genetic algorithm, eLEA3D) was adopted within the binding pocket of 6GGD and our ligand **DLIG1** was designed after several rounds of mutations. Docking and molecular dynamics (MD) simulation revealed significant interactions with key amino acid residues such as Cys220, Asp228, Leu145, Trp146, Val147, Thr150, Pro151, Pro152, Pro222, Pro223, Asp228, and Thr230. Along with sufficient binding stability, the MMGBSA analysis revealed its comparable binding free energy with other reported reference ligands (i.e. PK9324 and PK9318). Similar to these reference ligands, **DLIG1** exhibited specificity in binding towards the Y220C mutant rather than towards wild-type P53. Finally, **DLIG1** displayed a reorientation of a hydrophobic cavity in Y220C that hinted restoration of electrostatic interactions within the key loops of P53 favoring regain of its function.

ARTICLE HISTORY

Received 11 August 2022
Accepted 22 February 2023

KEYWORDS

Mutant P53; docking; molecular dynamics; MMGBSA; hydrophobic cavity

1. Introduction

The P53-mediated apoptotic pathway is a major pathway that is involved in the progression of cancer, with approximately 50% of human cancers arising due to mutations in the *p53* gene [1]. The P53 protein plays a significant role in suppressing unregulated cell division and is therefore referred to as a tumour suppressor [2,3]. In humans, the P53 phosphoprotein comprises 393 amino acids and has a molecular mass of 53 kDa, and is coded by the human *p53* gene located on chromosome number 17. The P53 protein typically comprises three functional domains, including an NH₂-terminal, trans-activation domain (TA; residues 1–63), a DNA-binding domain (DB; residues 102–292), and a COOH-terminal oligomerisation domain (OD; residues 319–359) [3,4].

The P53 gets immobilised by mutation in major cancer types with the point mutation of tyrosine in the 220th residue with cysteine (Y220C) affecting its DNA binding ability. The destabilisation of the DNA-binding domain leads to unfolding and aggregation due to the loss of thermostability and hydrophobic interactions [1,2,5–7]. In various cancer cases, tumour suppressor P53 gets inactivated by mutation and its function could be restored by binding to small molecule stabilisers [5]. Thus, small molecules could effectively bind to Y220C pocket and reactivate the mutant to provide a promising strategy for new anti-cancer therapeutics [5,6,8].

A literature survey suggests that the N-ethyl carbazole compound PK083 could be a potential stabiliser of the P53 mutant protein [1,2,5,7]. Similar promising mutant P53 stabilising activities have been reported for pyrrole-substituted pyrazole derivative PK7088 [5]. Carbazole derivatives substituted with 5-membered heterocycle have been acknowledged to increase binding affinity with P53 mutant by two folds resulting in restoration of its active tertiary structure and gain of function as guardian of the cell [1,5]. Oxazole-substituted carbazole (PK9318) is also reported to be a potent binder with Y220C variant of P53 and it was subsequently acknowledged to induce cell restoration activity in the liver cancer cell line. Similarly, thiophene substitution in carbazole resulted in another compound (PK9324) that also exhibited significant thermo-stabilisation of the mutant protein.

Various *in silico* methods such as fragment-based drug design and structure-guided molecular dynamics (MD) may help in designing such small molecule stabilisers. Thus, an in-depth analysis of Y220C binding site flexibility is performed first [9] and the 3D conformation of P53 protein is then utilised for the fragment-based design of potent small molecule. Herein, a carbazole-based fragment was selected as a template for *de novo* design of the lead molecule, the binding affinity of which was subsequently confirmed using robust computational methods, such as molecular docking (both flexible

and semi-rigid) and MD simulation analyses. The protein conformation change is a real dynamic change in physiological fluid that may be simulated by thermostatic, barostat, and periodic boundary conditions guided by MD simulation [10–12]. Therefore, MD simulation results are extremely important to analyze the actual dynamic protein–ligand interactions, the stability of protein–ligand complexes, any crucial conformational change of protein induced by ligand binding during simulation, free energy changes, and many others [10,11,13–17]. In addition to that, the drug-likeness properties and *in silico* toxicity of the ligand molecule were predicted and the top-scoring molecules were screened for hit identification.

2. Materials and methods

2.1. Materials

The protein structures were downloaded from the PDB (www.rcsb.org) and energy minimisation was subsequently performed with the help of Avogadro 1.2 (Free Software Foundation, Inc., Boston, USA) using the steepest descent algorithm and the Universal Force Field (UFF) [18]. The protein structures were tailored and analyzed in Discovery Studio Visualiser (Dassault Systems, BIOVIA, San Diego, USA) and UCSF Chimera (University of California, San Francisco). The prepared ligands were geometrically optimised in Avogadro 1.2 using the UFF and these were subsequently docked using AutoDock v4.2 and AutoDock FR (Scripps Research Institute, La Jolla, California, USA) [19,20]. The receptor–ligand interactions were evaluated in Discovery Studio Visualiser v3.2 (<https://discover.3ds.com/discovery-studio-visualizer-download>). Analyses of protein surface, hydrophobic clefts, and dipole moment calculations also were performed with this same tool. *De novo* ligand design was performed using e-LEA3D [21,22]. MD simulations [23] were performed using Desmond v5.2 (Desmond, Schrodinger, New York, USA) and Amber20 [24,25].

2.2. Mapping the common 3-D space of mutations in mutant P53

Mutant sequences were collected from The International Agency for Research on Cancer (IARC) TP53 database (<https://p53.iarc.fr/>). The common 3D space for mutations in breast cancer tumour protein P53 (TP53) [2,26,27] was analyzed by sequence alignment with fifty mutant P53 sequences using Clustal Omega and Box Shade. Box Shade mapping was used to mark the domain where the probability of mutations was calculated.

2.3. Retrieval of breast cancer-related mutant P53 from PDB

The PDB structure 6GGD is a mutant (Y220C) P53 protein bound to the ligand PK9324 (i.e. 9-ethyl-7-(1, 2-oxazole-4-yl)carbazol-3-yl methyl-methyl-azanium or EYB) (Figure 1) and this mutation is mainly related to breast cancer[8]. This co-crystallised ligand is already published in an earlier report [1] as a scaffold to restore the function of mutant P53 into

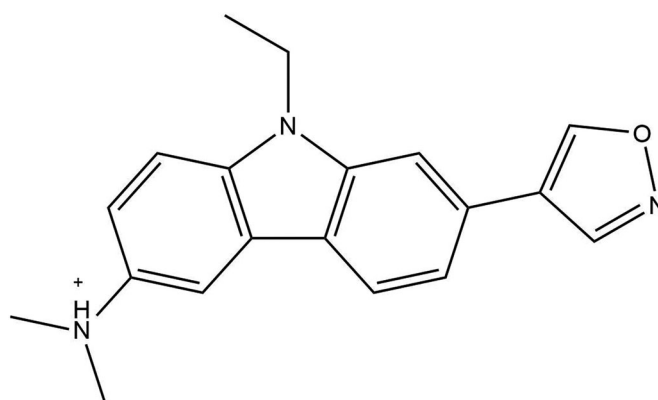


Figure 1. 2D structure of co-crystallised ligand (EYB) with 6GGD.

native P53 subsequently attenuating cell proliferation in certain carcinoma cells.

2.4. Validation of the docking method through redocking of the cocrystallised ligand

The PDB structure 6GGD was selected as the target macromolecule. The PDB structure of the protein was checked in PROCHECK and the model was refined in MODREFINER [28] to manage any artifacts present in the structure. The protein structure was then processed using PDB2PQR (<https://server.poissonboltzmann.org/pdb2pqr>) using the AMBER force field [29]. The prepared protein was processed in AutoDock Tools 4.0 (The Scripps Research Institute, LaJolla, California) by adding Kollman charges, merging non-polar hydrogen, and removing water molecules. A cubic grid was defined around the binding site of the ligand PK9324 in the PDB file 6GGD [20]. The dimensions of the grid along the x, y, and z axes were 50 × 50 × 50, respectively, and the grid spacing was 0.375 Å. The X, Y, and Z coordinates of the grid centre were 123.508, 105.167, and –44.452, respectively. The ligand was docked flexibly using the Lamarckian genetic algorithm, using 250 runs. The number of generations was 27,000 and the number of energy evaluations was set at 2,500,000. The rate of gene mutation was 0.02 and the crossover rate was 0.8. For studying convergence, the docked solutions were clustered using a clustering RMSD of 2.0 Å, and the lowest-scoring pose of the largest cluster was selected as the optimum solution. The binding affinity was reported in Gibb's free energy (ΔG) format and the binding interactions were determined with Discovery Studio Visualiser 3.5.

2.5. De novo ligand design

The binding site was defined from the grid map generated during the docking of the ligand–protein complex. The eLEA3D (with a license from <https://chemoinfo.ipmc.cnrs.fr/>) was used to generate various conformations of the ligand. In this process, the scaffold was allowed to hybridise with 7986 drug-like fragments stored in fragment library of LEA3D with an optimised condition for avoiding steric clashes and subsequently utilising the opportunity for covalent joining with user-defined hotspots onto a scaffold. Briefly, the process

was initiated by providing PK9324 as the template scaffold for *de novo*. The template was first docked by PLANTS (Protein Ligand-based Ant Colony Optimisation) onto the user-defined binding site of the protein and the best-docked conformations were reserved by the software. The best-docked conformations were concomitantly reprocessed by an inbuilt algorithm of LEA3D *via* mutating suitable fragments on the scaffold (deleting, adding, or changing it with other repository fragments by a coherent algorithm of the software). Each mutant, thus generated, was automatically redocked onto the protein. Subsequently, the best mutants classified by the improved docking scores were automatically selected by LEA3D. Next, those best 'mutants' were then crossed over with each other as per genetic algorithm to generate newer offspring. Each offspring which was nothing but a newly designed ligand was categorised by a 'fitness score'. The fitness score has been a weighted average of the docking score of the offspring and certain inbuilt topological functions calculated by FlexX as a part of LEA3D. Ten generations of evolution were performed keeping the population size as 20 molecules, crossover probability as 30%, and mutation probability at 70%. We have chosen the best-designed ligand with the best fitness score for subsequent studies.

2.6. MD simulation with desmond

The structure of the mutant P53-DLIG1 complex was initially prepared using the Protein Preparation Wizard in Schrödinger [30]. The protonation states of the protein were optimised using PROPKA at pH 7.0, and the water molecules within 3.0 Å of the hetero atoms were removed [31]. Following protein preparation, the system was prepared in Desmond by solvating the complex with the TIP3P solvent model in an orthorhombic box with a thickness of 10 Å from the edges of the protein. The solvated system was subsequently neutralised by the addition of 6 Cl⁻ ions, and the final concentration of the solution was set to 0.15 M by adding Na⁺ and Cl⁻ ions. The prepared system comprising 28,046 atoms was simulated for 100 ns using the OPLS4 force field in Desmond under the NPT ensemble [32]. The temperature was set to 310 K using the Nose-Hoover chain thermostat, and the pressure was set to 1.013 bar using the Martyna-Tobias-Klein barostat. The time step was set to 2.0 fs and periodic boundary conditions were used. The trajectory was visualised in Desmond, and trajectory analysis was performed using the Simulation Interactions Diagram module in Desmond [33].

2.7. MD simulation with amber

The ligand-receptor complexes were subjected to AMBER 20 for detailed MD investigation. The ligand parameterisation as well as the generation of topology (.top) and coordinate (.crd) files were carried out by using Leap script with the general AMBER forcefield and by utilising the auxiliary program Antechamber. The MD simulations were performed with the ff99SB forcefield in a cubic box of TIP3P explicit water with an 8 Å distance around the complexes. The positive charges were then neutralised with chloride ions. Subsequent MD simulation steps were described previously [34] and these are

not repeated here. The trajectory analyses for Amber-based MD simulation were performed using CPPTRAJ software to obtain the plots for root mean square deviation (RMSD), radius of gyration (RG), root mean square fluctuation (RMSF) as well as solvent accessible surface area (SASA) using QtGrace software (<https://sourceforge.net/projects/qtgrace/>). Additionally, trajectory analyses were also performed using CPPTRAJ module to determine the hydrogen bonding between the ligands and the binding site amino acid residues. The energy contributions of the binding site amino acid residues were computed using per residue-free energy decomposition method with the help of Amber MM-GBSA module. All energy components (van der Waals, electrostatic, polar solvation, and nonpolar solvation contributions) were calculated using 200 snapshots extracted from the last 10 ns MD trajectories.

3. Results

3.1. Retrieval of mutant P53 proteins from the IARC TP53 database and mapping mutation sites

A total of 50 mutant P53 proteins reported from various breast carcinomas were retrieved and their amino acid substitutions were inspected. The amino acid substitutions observed in various mutant P53 proteins were R249S, R175H, K132Q, Y163C, A138V, Y220C, etc [27,35,36]. Altogether, residues 125–285 were revealed as mutation hotspots for carcinogenic P53; so, any ligand perturbing this zone of mutant P53 is likely to combat the effects of mutations producing cancer (Figure 2).

3.2. Selection of mutant P53 and template ligand

The Y220C mutation has been selected since this mutation has been one of the most frequent mutations in P53 and it appears in 1,00,000 cases per year [1]. Ligand PK9324 was selected as the template ligand based on the fact that earlier reports have shown that carbazole-based template ligand could be an excellent scaffold to combat the Y220X type of mutation in mutant P53 [1]. However, due to the presence of two neighbouring heteroatoms in the five-membered heterocycle attached as side chain with this ring, the authors reported that PK9324 suffers from low thermostability and thus results in weaker binding with the Y220C mutant protein [1]. Thus, it is pertinent to assume that this ligand needs improvisation in terms of binding affinity and stability, hence requiring certain engineering as next stage of ligand design. However, PK9324 satisfies the primary criteria for being a template ligand first by covering the Y220C mutation upon docking (Figure 3) and second, by interacting with the amino acids in the hotspot region of residue 125–285 in mutant P53.

3.3. De novo ligand design

From the generation of *de novo* ligands by eLEA3D, ligands were first screened based on the fitting function, and the ligands bearing poor fitting functions and/or redundant structures were eliminated. Eighteen (18) ligands (Table S1) were selected based on their improved fitting score inside the

```

BAC16799.1 P53 [Homo sapiens]
MEEPQSDPSVEPPLSQETFSDLWKLLPENNVLSPLPSQAMDDLMLSPDDIEQWFTEDPGPDEAPRMPEAAPRVAPAP
AAPTPAAPAPAPSWPLSSSVPSQKTYQGSYGFRLGFLHSGTAKSVTCTYSPALNKMFCQL
AKTQPVQLWVDSTPPPGRFRAMAIYKQSQHMTEVVVRCPPHHERCSDSDGLAPPQHLIRV
EGNLRVEYLDDRNTFRHSVVVPYEPPEVGSDDCTTIHYKYMCSYSSCMGMNRRPILTIITL
EDSSGNLLGRNSFEVHVACACPRDRRTEENLRKKGEPHHELPPGSTKRALSNNNTSSSPQ
PKKKPLDGEYFTLQIRGRERFEMFRELNEALELKDQAQKEPGGRAHSSHLKSKKQST
SRHKKLMFKTEGPDS

```

Figure 2. (Colour online) Hotspot zone of P53 mutation responsible for cancer as revealed by sequence alignment of selected 50 mutants on breast cancer from TP53 database.

binding site and non-redundancy in their structures. The ligands were re-docked to the binding site of 6GGD using AutoDock v 4.2 and it was found that the binding affinities of ligands 1, 10, 11, 13, 14, 18 are -8.6 , -8.8 , -8.7 , -9.0 , -8.9 and -9.5 kcal/mol, respectively. Apart from Ligand 14, other ligands showed more violations of drug likeliness (Lipinski's rule of five, Veber rule) or more toxicity or lesser synthetic accessibility (ADMET SAR). Ligand 14 exhibited better acceptability in all those parameters and at the same time, it retained a good binding score showing satisfactory interactions with the mutated protein. This ligand was designated as **DLIG1** and was chosen as a template ligand for further studies [2].

3.4. Binding interactions obtained from *in silico* docking studies

The designed ligand DLIG1 could interact with the hotspot mutation zone similar to PK9324 which has several common binding residues with the mutant P53 (6GGD), including Cys220 (site of P53 mutation), Val147, Asp228, Pro220, Pro223, Thr230 and Pro153 [1,7]. Noticeably, all these residues fall within the hotspot region (residues 125-185) that belongs to the DNA binding domain, and this region contains most of the carcinogenic P53 mutations as reported in previous studies [4]. Therefore, it may be assumed that the modelled ligand can interact with all the residues in the hotspot zone.

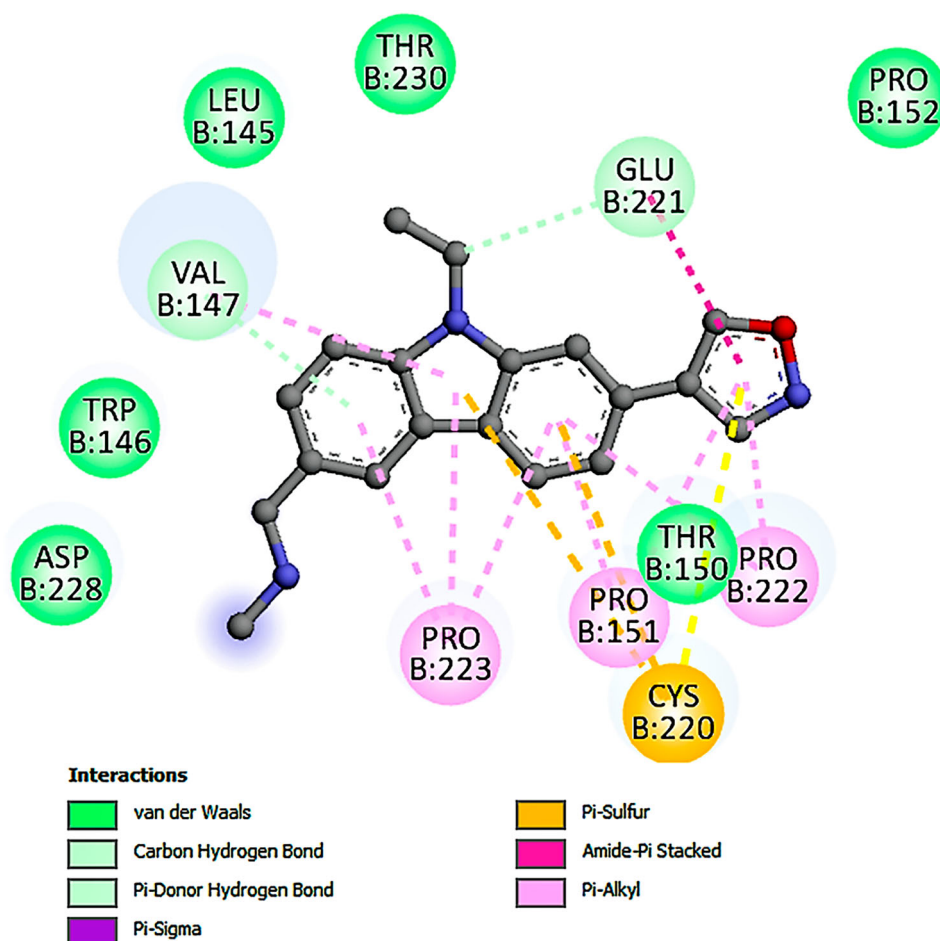


Figure 3. (Colour online) Binding site interactions of an inbound ligand with 6GGD.

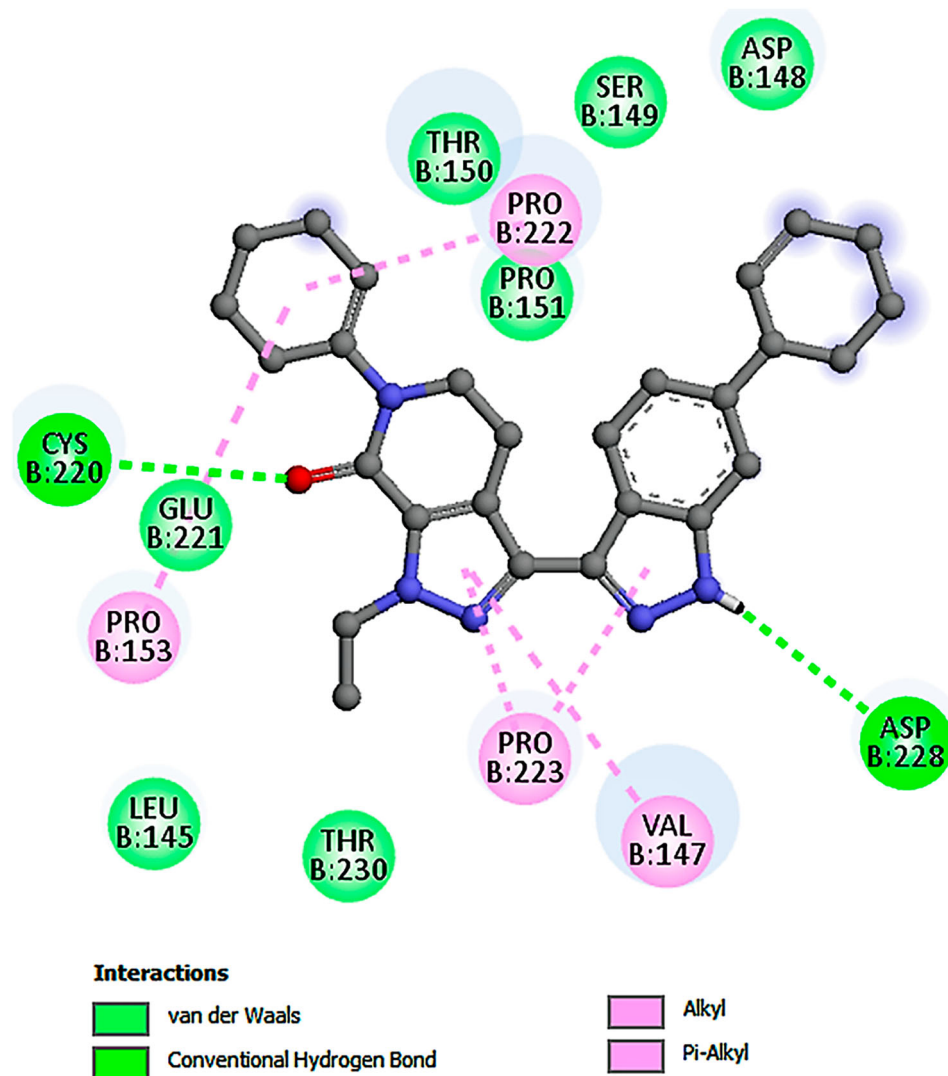


Figure 4. (Colour online) Docked pose of the ligand within the binding pocket of 6GGD and 2D interaction between **DLIG1** and spanning binding site residues.

It especially reinforces the interactions between Cys220, Val147, Pro153, Pro222, and Pro223 [3,4] and establishes interactions such as hydrogen bonding with hydrophilic Asp228 within the dipped sub-site (Figure 4).

An additional flexible docking by AutoDock FR (ADFR suite 1.0, <http://adfr.scripps.edu/AutoDockFR>) revealed that the flexibility of the amino acid residues conferred more stability, fitting, and interactions with the ligand. When reference ligand PK9324 and our ligand **DLIG1** were compared to investigate their effects on the hydrophobic pocket created by Y220C mutation, both PK9324 (Figure 5(A)) and **DLIG1** (Figure 5(B)) have been observed to produce a similar kind of orientation of Cys220, Pro222, Leu145, Trp146, Val147, Thr150, Pro151, Pro152, Pro222, Pro223, Asp228 and Thr230. Therefore, it can be expected that a similar kind of loop restoration, refolding, and gain of function of P53 can be achieved by **DLIG1** as that of PK9324. A further investigation of the anatomy of the hydrophobic cleft in between S3/S4 and S7/S8 proximal loops [2] of 6GGD revealed that **DLIG1** aligns themselves in the hydrophobic cavity in Y220C mutant in such a way that the side chain of Cys220 rotates itself towards the ligands (Figure 5(B)), hydrogen

bond distance 2.95 Å) instead of the hydrophobic cavity of the protein [36,37]. Similar to PK9324, this designed ligand is likely to minimise the length of the hydrophobic pocket and would bring the hydrophilic amino acids closer for loop refolding.

One question that remains relevant is whether the designed ligand may possess selectivity towards the mutated Y220C P53 as compared to the wild-type P53. Bauer et al addressed the same question for the ligand PK9318 by simply superimposing the structure of the Y220C-PK9318 complex with the wild-type structure (PDB entry 2XWR) that led to the finding that Tyr220 of wild-type P53 blocks the structure of PK9318 whereas due to less bulky side chain, the Cys220 of Y220C P53 allows this ligand to occupy the same cavity without any steric hindrance [1]. In the current work, we performed a similar experiment by superimposing 6GGD structure with 2XWR and the result is shown in Figure 6. The Bulky aromatic side chain of Tyr220 blocks PK9324 (bound ligand of 6GGD). Similarly, the docked complex of **DLIG1** (with 6GGD) was also superimposed with 2XWR and a steric clash between Tyr220 and **DLIG1** was noticed. Therefore, it may be assumed that similar to PK9324, our designed ligand should also have

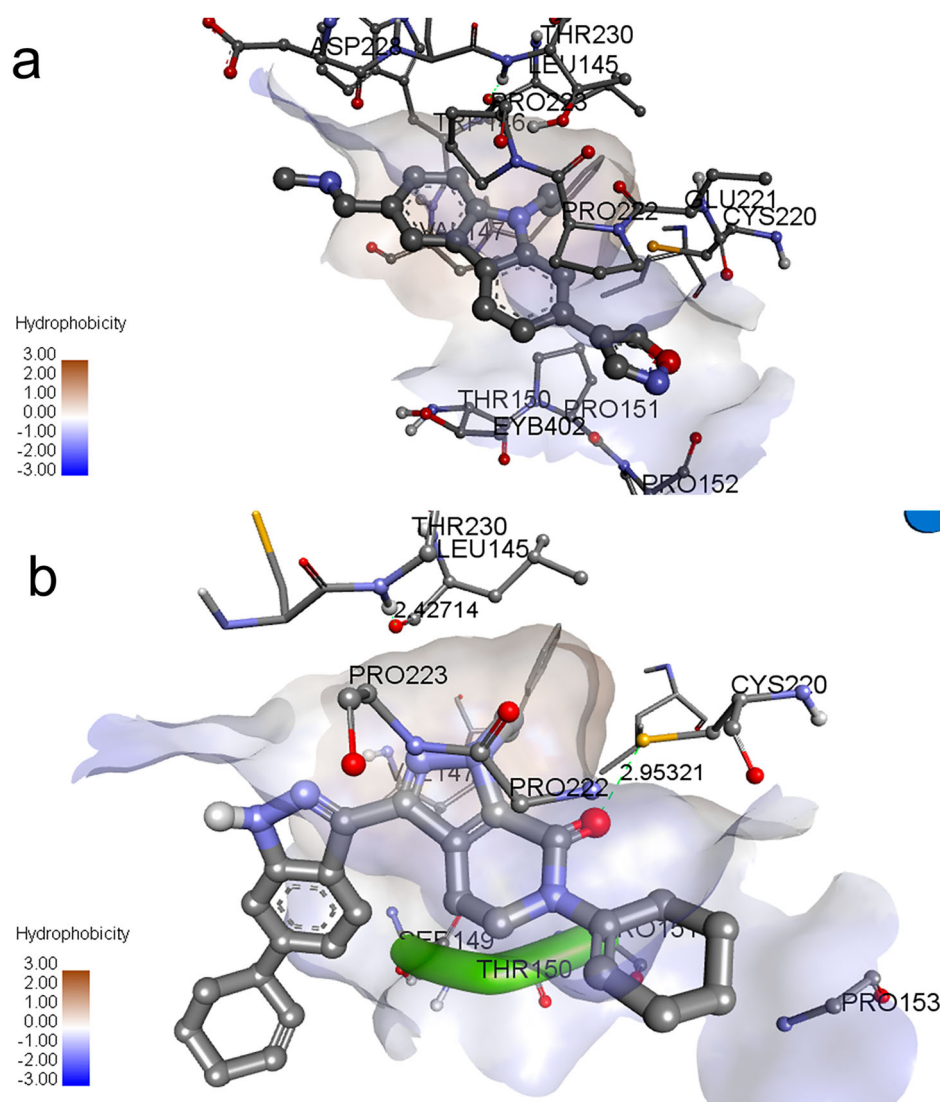


Figure 5. (Colour online) Re-orientation of the hydrophobic cleft within 6GGD in between S3/S4 and S7/S8 loops. (A) After PK9324 binding (B) After DLIG1 binding.

selectivity towards the mutated p53 as compared to wild-type P53. Nevertheless, we went a step further to reassure this assumption and docked the structures of PK9324 and DLIG1 at the specific binding site of the 2XWR. Significantly, no docked pose was retrieved at the binding cavity containing Tyr220. This may further justify that both PK9324 and DLIG1 should selectively inhibit the mutated P53.

3.5. MD simulations

3.5.1. Target structure validation and initial stability check of the ligand–protein complex

MD simulations were performed for checking the stability of the ligand–protein complex in a real–period [38–40]. The DOPE score of the protein after filling in the missing residues was -39114.15234 whereas the GA341 score was 1, indicating satisfactory model reliability. The normalised QMean4 score of the modelled protein was 0.35 which falls within the range of values for the non-redundant set proteins of similar size in the PDB.

Initially, a 100 ns MD simulation was carried out using Desmond software, which is a relatively faster tool, to understand

the binding stability of the DLIG1-6GGD complex. As observed from RMSD plots of Figure 7, both the protein–complex and ligand reached sufficient stabilities during the 100 ns MD simulation run.

After confirming this from Desmond, detailed MD simulation analyses were performed with Amber software, and this time, not only DLIG1-6GGD but two other complexes namely 6GGD-PK9318 and 6GGD-PK9324 were also subjected to 100 ns MD simulation for comparative analyses. These MD simulations indicate that the 6GGD-DLIG1 complex exhibits similar fluctuations as compared to 6GGD-PK9318 as their RMSD values were within 2.5 Å throughout the 100 ns run. Furthermore, the 6GGD-PK9324 displayed deviations within the 3 Å range (Figure 8(a)). The ligand RMSD was also checked to observe the fluctuations of the protein complexes in the presence of ligands. The RMSDs of bound ligands were less than 2.0 Å confirming that the ligands have been stabilised at their binding sites (Figure 8(b)).

The ligands of 6GGD-PK9318 and 6GGD-DLIG1 unveil preferable stabilities as compared to that of 6GGD-PK9324 [41]. Additionally, a radius of gyration (Figure 9(a)) and

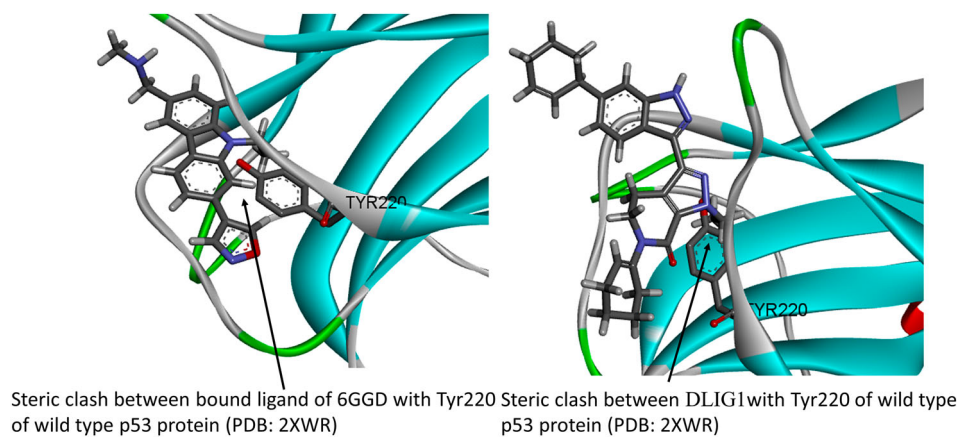


Figure 6. (Colour online) The steric clashes between the PK9324 and DL1G1 with Tyr220 of wild-type p53 protein.

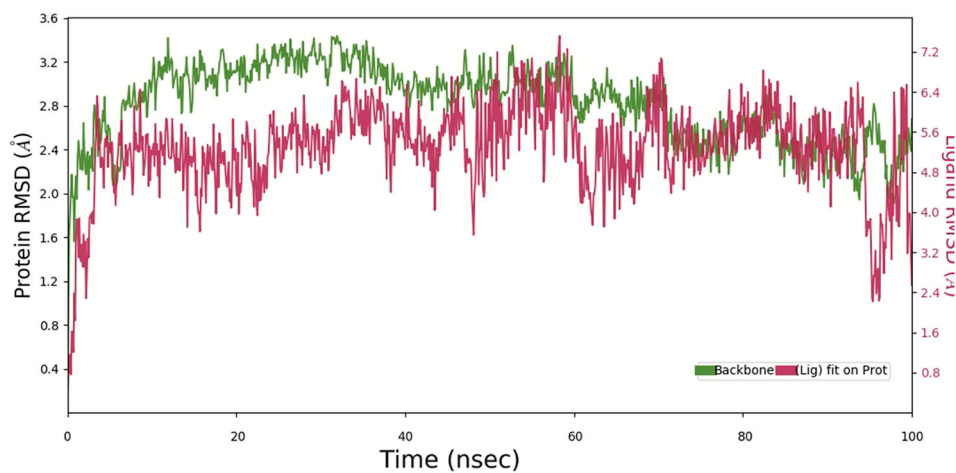


Figure 7. (Colour online) RMSD values of the protein backbone atoms (green) and DL1G1 (red) fitted to the protein, during the 100 ns production run.

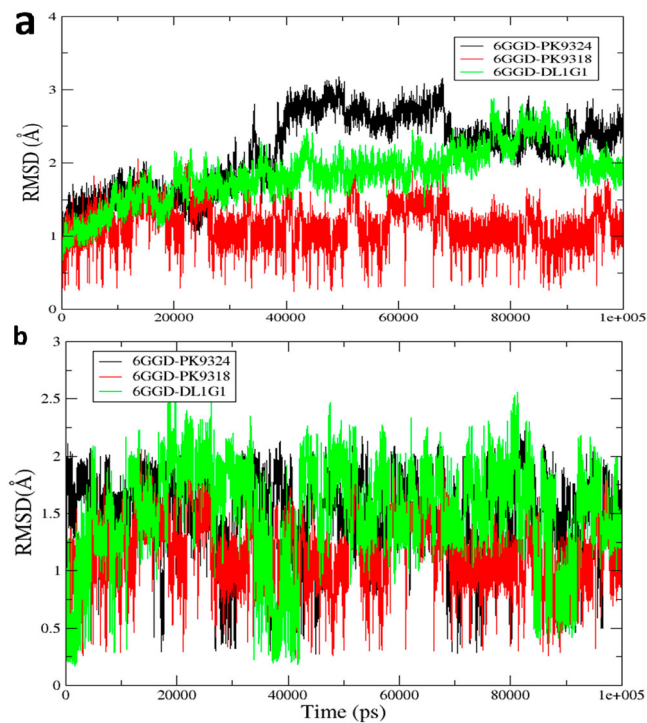


Figure 8. (Colour online) (a) RMSD plots of protein complexes and (b) RMSD plots of ligands in 100 ns MD simulations.

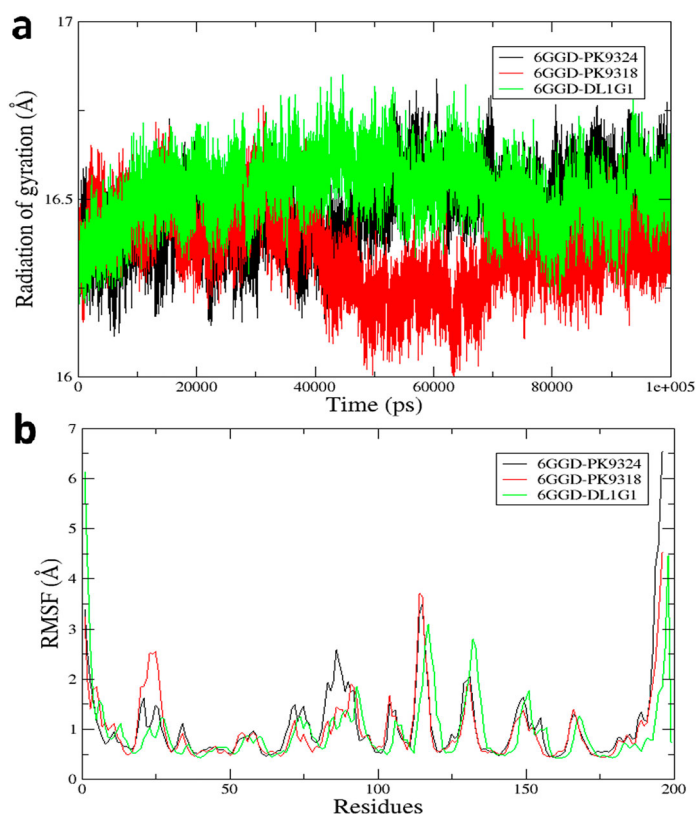


Figure 9. (Colour online) (a) Radius of gyration plots and (b) RMSF plots of protein complexes.

RMSF (Figure 9(b)) plots of the above complexes indicate that the dynamic behaviour of 6GGD-DLIG1 is more comparable to 6GGD-PK9318 than 6GGD-PK9324. The radius of gyration plots indicated sufficient rigidity of all these three complexes. In addition to these, we also determined the solvent-accessible surface area (SASA) of the 6GGD-DLIG1 (results presented in Supplementary materials, Figure S1) and it was found to be stable during the MD simulation run.

The binding free energies ($\Delta G_{\text{bind}}(T)$) of PK9318 in the 6GGD-PK9318 complex was -21.09 kcal/mole and that of PK9324 in the 6GGD-PK9324 complex was -15.17 kcal/mole confirming our scope of study (Table 1). Additionally, ($\Delta G_{\text{bind}}(T)$) of the DLIG1 complex was found to be higher than 6GGD-PK9324 but lower than 6GGD-PK9318. Thus, these results suggest that the DLIG1 may be a potential candidate to bind with the Y220C mutant P53.

Furthermore, per residue decomposition analyses were performed with amino acid residues of the binding cavity to understand the free energy contributions of these residues for binding of DLIG1 [42]. Docking studies insinuated van der Waals interactions with Cys 229, Cys 220, and Thr 230 (Figure 4). Noticeably, these interactions are comparable to the results from per residue decomposition analysis

(Figure 10). The residues falling under the hotspot region were Val147, Asp228, Pro222, Pro223, and Pro153, which exhibited majorly van der Waals interactions. Interestingly, the highest electrostatic interactions were observed for Cys220. The Trp146 and Pro151 exhibited proportional electrostatic interactions (Figure 10).

Stabilisation of Y220C complex bound with the designed ligand was reflected by observing the distance fluctuations in specific residues of the DNA binding domain region of P53 protein [7]. The rotameric shift of the side chain of Cys220 was found to be oriented towards the bond vector, exactly opposite to that observed in the *apo* structure. It may be due to the strong electronic field of the ligand, onto mutant P53 [2,43]. In certain instances, Cys220 side chain gets flipped and the sulfhydryl group points away from the central cavity which in turn increases the depth of the binding cavity by reaching near the hydrophobic residues namely, Leu145 and Leu257. The distance fluctuations concerning nanosecond time frame between Cys220 and the two hydrophobic residues Leu145 and Leu257 are explored to observe if there is any decrease in the depth of binding cavity. The Cys220-Leu145 or Cys220-Leu257 distance remains close to the distance values of 6GGD-PK9318

Table 1. Calculated binding free energies [$\Delta G_{\text{bind}}(T)$] of the complexes. The energy components are in Kcal/mole.

Complexes	ΔE_{vdW}	ΔE_{elec}	ΔG_{gas}	ΔG_{polar}	$\Delta G_{\text{nonpolar}}$	$\Delta G_{\text{solvation}}$	$-T\Delta S$	$\Delta G_{\text{bind}}(T)$
6GGD-PK9324	-45.35	-113.58	-158.93	125.72	-4.74	120.98	-22.78	-15.17
6GGD-PK9318	-41.91	-95.6	-137.52	101.48	-4.42	105.92	-14.95	-21.09
6GGD-DLIG1	-45.18	-3.67	-48.85	16.21	-4.77	11.43	-20.03	-17.39

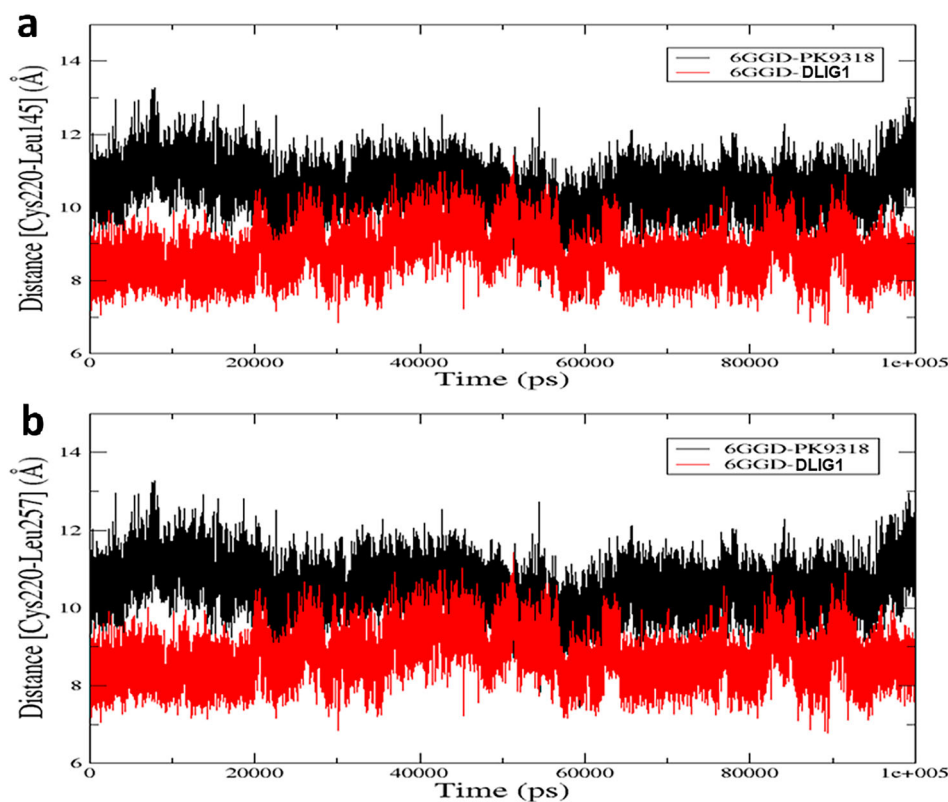


Figure 11. (Colour online) Distance fluctuations in (a) Cys220-Leu145 (b) Cys220-Leu257 in comparison to 6GGD-PK9318.

throughout the MD simulation study (Figure 11). This points out that the state of the central cavity does not change in a real time frame.

3.6. Drug-likeness and ADME screening

The drug-likeness and ADME prediction by SWISS ADME revealed the compound DNLIG1 bears favorable pharmacokinetic properties. For example, it passes most of the drug likeliness rules such as Lipinsky, Veber, Muegge, and Egan rules to pass as a promising drug candidate (Table 2). It is likely to pass through the gastrointestinal tract and its bioavailability score is moderate (0.55). Although it may inhibit some variants of cytochromes (CYP2C19, CYP2C9, CYP3A4), it acts as a non-inhibitor for CYP1A2 and CYP2D6. These results indicate that DLIG1 outlays a potential scaffold for future applications.

3.7. Toxicity prediction

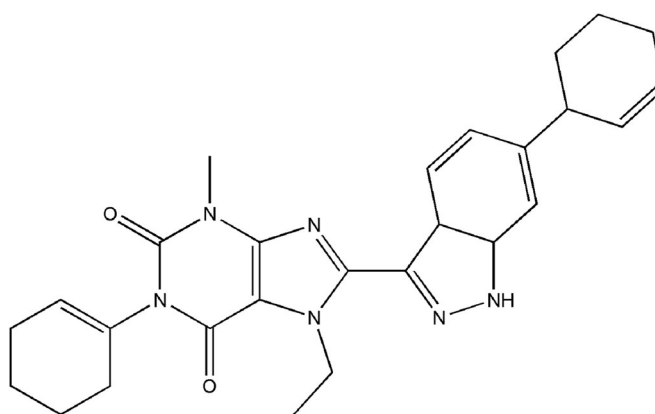
In addition, a comparative toxicity study between the reference ligand (PK9324) and DLIG1 revealed a similar toxicity profile *in silico* (ADMET SAR, Table S2). On further optimisation, it was found that the Optimised ligand (OptLIG1), with a little variation of its chemical structure, reduced toxicity drastically (Table S2). Aromatase binding and cytochrome inhibition (CYP1A2 to CYP3A4) were drastically reduced for OptLIG1 (Figure 12). Therefore, DLIG1 may be projected as a promising scaffold for designing with lower toxicity.

4. Discussion

Although a lot of attempts have been undertaken for the last few decades to develop anticancer drugs, the inadequacy of the currently marketed products to cure malignancies and uncontrolled cell proliferation indicates that the design of a novel anticancer agent is of utmost requirement. Hence it becomes pertinent to undertake an attempt for designing a newer scaffold as an anticancer agent by logical and validated arrays of drug design. In this kind of design, it becomes very important to choose a target for drug design. Herein we have chosen Y220C mutant P53 since it is the ninth most frequent mutation responsible for cancer as revealed by TP53 database and more than 1,00,000 reported cases are published every year with this mutant P53 being the key player for carcinogenesis [26]. Furthermore, previous reports acknowledged that the leading cause of mutant P53-guided oncogenesis has been its loss of 'protecting' function against abnormal cell proliferation *via* MDM2-P53-P63/P73 check loop [26]. A more deep insight into the problem revealed that Y220C mutation leads to disruption of the P53 tertiary structure especially elongating a hydrophobic cleft into its binding sites or subsites hence breaking electrostatic interactions between S3 and S4 loops as well as S7 and S8 loops consisting of Val147, Pro151, Pro153, Pro223 amino acids [5,7,44]. Hence one of the keys to ingrestoring the imbalance of function of mutant P53 is to restore these interactions by reducing the depth and diameter of the hydrophobic cleft, bringing loops closer, and allowing them to reinforce bonds with each other. A handful of literature are published in this field, amongst them Bauer et al reported a cluster of amino carbazole derivatives that have

Table 2. ADME and drug-likeness prediction of **DLIG1** by SWISS ADME.

Formula	C27H35N5O
MW	445.6
#Heavy atoms	33
#Aromatic heavy atoms	6
Fraction Csp3	0.56
#Rotatable bonds	4
#H-bond acceptors	3
#H-bond donors	2
MR	151.17
TPSA	59.97
iLOGP	3.82
XLOGP3	5.25
WLOGP	2.43
MLOGP	3.79
Silicos-IT Log P	3.19
Consensus Log P	3.7
ESOL Log S	-5.78
ESOL Solubility (mg/ml)	0.000738
ESOL Solubility (mol/l)	1.66E-06
ESOL Class	Moderately soluble
Ali Log S	-6.26
Ali Solubility (mg/ml)	0.000246
Ali Solubility (mol/l)	5.51E-07
Ali Class	Poorly soluble
Silicos-IT LogSw	-5.39
Silicos-IT Solubility (mg/ml)	0.0018
Silicos-IT Solubility (mol/l)	4.04E-06
Silicos-IT class	Moderately soluble
GI absorption	High
BBB permeant	Yes
Pgp substrate	Yes
CYP1A2 inhibitor	No
CYP2C19 inhibitor	Yes
CYP2C9 inhibitor	Yes
CYP2D6 inhibitor	No
CYP3A4 inhibitor	Yes
log Kp (cm/s)	-5.29
Lipinski #violations	0
Ghose #violations	1
Veber #violations	0
Egan #violations	0
Muegge #violations	1
Bioavailability Score	0.55
PAINS #alerts	0
Brenk #alerts	1
Leadlikeness #violations	2
Synthetic Accessibility	5.65

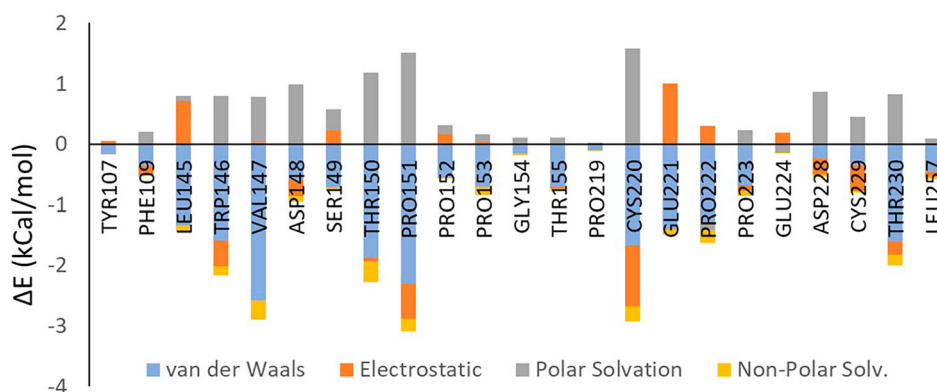
**Figure 12.** (Colour online) Optimised ligand (OptLIG1) with reduced toxicity.

reported in PDB as ligand EYB within Y220C variant of P53 (PDB ID: 6GGD). Since our docking validation demonstrated significant interaction of PK9324 with Cys220 together with other amino acids at P53 hotspots of mutation (res125-res185), the same was chosen as a scaffold for new compound design against the P53 variant.

In pursuit, *de novo* ligand design using a genetic algorithm within the binding site of 6GGD yielded 18 non-redundant and fundamental ligands which showed a good amount of fitting and docking energies *de novo*. Re-docking the *de novo* ligands via AutoDock 4.2 against 6GGD, led to the selection of **DLIG1** based on its binding affinity and interactions with the binding site residues. A significant number of binding residues match between the template (PK9324) as well as **DLIG1** suggesting similar Y220C antagonistic activity in mutant P53, in other words, advocating the same restoration potential of the mutant protein.

A further MD simulation-based analysis and modelling revealed that several bonds within **DLIG1** are rotatable rendering it conformational flexibility which marked its strength to fit within the binding cavity of 6GGD. Further analysis of SASA, PSA, RMSD, and RMSF all preached the stability of **DLIG1** within the binding pocket advocating its longer duration of action in the cell. Moreover, PK9324 and PK9318 being subjected to MD simulations as positive controls, the Rg and RMSF revealed better stability of **DLIG1**-P53 complex than PK9324-P53 but comparable to PK9318-P53 complex.

been computationally and experimentally proven to restore P53 function and dampen oncogenesis [1,7,45,46]. Among them, PK9318 and PK9324 have been reported as two potential inhibitors of Y220C variant, of which PK9324 has been

**Figure 10.** (Colour online) Per-residue decomposition profiles of **DLIG1** complex with Y220C mutant P53.

Now, a crucial question comes herein could **DLIG1** reduces the hydrophobic cleft inside the host and reintroduce the S3/S4 and S7/S8 interactions? To address that, we have considered a potential PK9318 ligand from the published reports of the same Bauer group, that has been used to achieve a significant restoration of a non-functional P53 mutant into a functional one. Since the Cys220-Leu145-Leu257 triangle portrays the major bury of hydrophobic cleft inside mutant P53, we undertook MD simulation-based distance analyses between Cys220-Leu145 and Cys220-Leu257 for both PK9318-P53 and DLIG1-P53 complex [1]. Interestingly, it was noted that distance fluctuations during 100 ns simulation were almost similar for both the complexes thus implying that the geometrical alteration of loop space of DLIG1-P53 is very comparable with that of PK9318-P53 complex. Hence a similar effect of protein structure alteration (involving re-introduction of crucial loop-loop interactions) could be expected for DLIG1-P53 as that of PK9318-P53 complex. Not only that but also lowering of the dissociation constant (Kd), enhancement of melting temperature of P53 (Tm), downstream activation of anticancer genes by PK9318-P53 complex, as reported by Bauer et al [1,2,7] might be anticipated for DLIG1-P53 complex as well.

In addition, by the chemical superimposition of another ligand SLMP53-1 [7,47] (reported to revert mutant P53 into native P53 subsequently reducing P53 expressing tumours) onto the structure of **DLIG1**, it was found that **DLIG1** and SLMP53-1 bear more than 0.5 coefficient of similarity (Discovery Studio Visualiser) where Benz pyrazole of **DLIG1** (C20-N11, N12) and Benz pyrrole (C22-N12) of SLMP53-1 almost merged (Figure S2). It suggests that the aromatic hydrophobic head and electron acceptors of both scaffolds bear significant structural resemblance with others. Furthermore, the pyrazole ring of N-piperidine pyrazole in **DLIG1** holds similar chemical space (atom to atom distance 1.7 Å) with the second pyrrole ring of SLMP53-1 attached to the second benzene ring. The notable structural resemblances between SLMP53-1 and **DLIG1** lead to the assumption that they may likely exert similar binding pattern within mutant P53 and finally bringing in similar downstream effect.

5. Conclusion

In this study, we have designed a ligand, **DLIG1** by *de novo* and docking-based ligand design against mutant P53 that could restore the gain of function within the mutant *via* possible restoration of the native conformation of P53. The ligand establishes van der Waals interactions between Cys220, Val147, Pro153, Pro222, and Pro223; together with introducing hydrogen bonding with Asp228 within the central cavity and sub-site2 of P53 protein. The ligand reaches the hydrophobic pocket created between the S3/S4 and S7/S8 loops by the Cys220 mutation in native P53 of cancerous cells. The hydrophobic regions in the ligands are the key contributors to the ligand-receptor interaction. We, therefore, selected **DLIG1** as a hit against the mutant P53 (PDB ID: 6GGD). Additionally, binding site analyses revealed that the ligand interacted with the most vulnerable mutation zone in P53 (residues 128–285). The MD simulations study demonstrated that the ligand **DLIG1** did not dissociate from the binding

pocket during 100 ns simulation. We presume that ligands with such rotational and torsional flexibility can preoccupy the relevant site of the protein. The RMSD, RMSF, and radius of gyration values confirmed the adequacy of hydrogen bonds with the residues spanning the binding site, thus suggesting that the **DLIG1** could form stable interactions with the Y220C mutant P53. The DLIG1-6GGD complex exhibited comparable fluctuations of Cys220-Leu145 distance or Cys220-Leu257 distance to that of 6GGD-PK9318 signifying similar alternations of the hydrophobic cleft within the mutant by both the ligands. Hence, in a nutshell, the **DLIG1** ligand may be considered as a promising scaffold for designing novel lead compounds against cancer caused by mutant P53.

Acknowledgements

The authors express their gratitude to Dr. B.C. Roy College of Pharmacy & Allied Health Sciences, Durgapur, WB, India for providing the required infrastructure for the project.

Disclosure statement

No potential conflict of interest was reported by the author(s).

References

- [1] Bauer MR, Jones RN, Tareque RK, et al. A structure-guided molecular chaperone approach for restoring the transcriptional activity of the p53 cancer mutant Y220C. *Future Med Chem.* 2019;11:2491–2504.
- [2] Rauf SMA, Endou A, Takaba H, et al. Effect of Y220C mutation on p53 and its rescue mechanism: a computer chemistry approach. *Protein J.* 2013;32:68–74.
- [3] Ozaki T, Nakagawara A. Role of p53 in cell death and human cancers. *Cancers (Basel).* 2011;3:994–1013.
- [4] Bullock AN, Henckel J, Fersht AR. Quantitative analysis of residual folding and DNA binding in mutant p53 core domain: definition of mutant states for rescue in cancer therapy. *Oncogene.* 2000;19:1245–1256.
- [5] Baud MGJ, Bauer MR, Verduci L, et al. Aminobenzothiazole derivatives stabilize the thermolabile p53 cancer mutant Y220C and show anticancer activity in p53-Y220C cell lines. *Eur J Med Chem [Internet].* 2018;152:101–114. doi:10.1016/j.ejmech.2018.04.035.
- [6] Chowdhury MR, Tiwari A, Dubey GP. In silico investigation of Y220C mutant p53 for lead design. *bioRxiv.* 2019.
- [7] Bauer MR, Krämer A, Settanni G, et al. Targeting cavity-creating p53 cancer mutations with small-molecule stabilizers: the Y220X paradigm. *ACS Chem Biol.* 2020;15:657–668.
- [8] Synnott NC, Bauer MR, Madden S, et al. Mutant p53 as a therapeutic target for the treatment of triple-negative breast cancer: pre-clinical investigation with the anti-p53 drug, PK11007. *Cancer Lett [Internet].* 2018;414:99–106. doi:10.1016/j.canlet.2017.09.053.
- [9] Rajendran V, Sethumadhavan R. Drug resistance mechanism of PncA in Mycobacterium tuberculosis. *J Biomol Struct Dyn.* 2014;32:209–221.
- [10] Rajendran V. Structural analysis of oncogenic mutation of isocitrate dehydrogenase 1. *Mol Biosyst.* 2016;12:2276–2287.
- [11] Kumar S, Bhardwaj VK, Singh R, et al. Identification of acridine-dione scaffolds as potential inhibitor of DENV-2 C protein: An in silico strategy to combat dengue. *J Cell Biochem.* 2022;123:935–946.
- [12] Bhardwaj VK, Oakley A PR. Mechanistic behavior and subtle key events during DNA clamp opening and closing in T4 bacteriophage. *Int J Biol Macromol [Internet].* 2022;208:11–19. doi:10.1016/j.ijbiomac.2022.03.021.

- [13] Singh R, Bhardwaj VK. Identification of 11 β -HSD1 inhibitors through enhanced sampling methods. *Chem Commun (Camb)*. 2022;58:5005–5008.
- [14] Rajendran V, Gopalakrishnan C, Sethumadhavan R. Pathological role of a point mutation (T315I) in BCR-ABL1 protein – a computational insight. *J Cell Biochem*. 2018;119:918–925.
- [15] Vijay Kumar Bhardwaj RP. A lesson for the maestro of the replication fork: targeting the protein-binding interface of proliferating cell nuclear antigen for anticancer therapy. *J Cell Biochem*. 2022;123:1091–1102.
- [16] Rajendran V, Purohit R, Sethumadhavan R. In silico investigation of molecular mechanism of laminopathy caused by a point mutation (R482W) in lamin A/C protein. *Amino Acids*. 2012;43:603–615.
- [17] Rajendran V, Gopalakrishnan C, Purohit R. Impact of point mutation P29S in RAC1 on tumorigenesis. *Tumor Biol* [Internet]. 2016;37:15293–15304. doi:10.1007/s13277-016-5329-y.
- [18] Hanwell MD, Curtis DE, Lonie DC. Avogadro: An advanced semantic chemical editor, visualization, and analysis platform. *J Cheminform*. 2012;4:1–17.
- [19] Morris GM, Huey R, Lindstrom W, et al. Software news and updates AutoDock4 and AutoDockTools4: automated docking with selective receptor flexibility. 2009.
- [20] Forli S, Huey R, Pique ME, et al. 00006565-201002000-00017. 2016;11:905–919.
- [21] Douguet D, Munier-Lehmann H, Labesse G, et al. LEA3D: a computer-aided ligand design for structure-based drug design. *J Med Chem*. 2005;48:2457–2468.
- [22] Douguet D. e-LEA3D: A computational-aided drug design web server. *Nucleic Acids Res*. 2010;38:615–621.
- [23] Alonso H, Bliznyuk AA, Gready JE. Combining docking and molecular dynamic simulations in drug design. *Med Res Rev*. 2006;26:531–568.
- [24] Roe DR, Cheatham TE. PTRAJ and CPPTRAJ: software for processing and analysis of molecular dynamics trajectory data. *J Chem Theory Comput*. 2013;9:3084–3095.
- [25] Wang J, Wolf RM, Caldwell JW, et al. 20035_Ftp. *J Comput Chem*. 2004;56531:1157–1174.
- [26] Chasov V, Mirgayazova R, Zmievskaya E, et al. Key players in the mutant p53 team: small molecules, gene editing, immunotherapy. *Front Oncol*. 2020;10:1–10.
- [27] Mantovani F, Collavin L, Del Sal G. Mutant p53 as a guardian of the cancer cell. *Cell Death Differ* [Internet]. 2019;26:199–212. doi:10.1038/s41418-018-0246-9.
- [28] Xu D, Zhang Y. Improving the physical realism and structural accuracy of protein models by a two-step atomic-level energy minimization. *Biophys J* [Internet]. 2011;101:2525–2534. doi:10.1016/j.bpj.2011.10.024.
- [29] Dolinsky TJ, Nielsen JE, McCammon JA, et al. PDB2PQR: an automated pipeline for the setup of Poisson-Boltzmann electrostatics calculations. *Nucleic Acids Res*. 2004;32:665–667.
- [30] Madhavi Sastry G, Adzhigirey M, Day T, et al. Protein and ligand preparation: parameters, protocols, and influence on virtual screening enrichments. *J Comput Aided Mol Des*. 2013;27:221–234.
- [31] Olsson MHM, Søndergaard CR, Rostkowski M. PROPKA3: consistent treatment of internal and surface residues in empirical pK_a predictions. *J Chem Theory Comput*. 2011;7:525–537.
- [32] Lu C, Wu C, Ghoreishi D, et al. OPLS4: improving force field accuracy on challenging regimes of chemical space. *J Chem Theory Comput*. 2021;17:4291–4300.
- [33] Bowers KJ, Chow E, Xu H. Scalable algorithms for molecular dynamics simulations on commodity clusters. *Proc 2006 ACM/IEEE Conf Supercomput SC'06*. New York, New York, USA: ACM Press; 2006. p. 84.
- [34] Halder AK, Cordeiro MNDSC. Multi-target in silico prediction of inhibitors for mitogen-activated protein kinase-interacting kinases. *Biomolecules* [Internet]. 2021;11:1670. DOI:10.3390/biom11111670.
- [35] Blandino G, Di Agostino S. New therapeutic strategies to treat human cancers expressing mutant p53 proteins. *J Exp Clin Cancer Res*. 2018;37:1–13.
- [36] Sundar D, Yu Y, Katiyar SP, et al. Wild type p53 function in p53^{Y220C} mutant harboring cells by treatment with Ashwagandha derived anticancer withanolides: bioinformatics and experimental evidence 06 biological sciences 0601 biochemistry and cell biology 11 medical and health S. *J Exp Clin Cancer Res*. 2019;38:1–14.
- [37] Campanera JM, Pouplana R. MMPBSA decomposition of the binding energy throughout a molecular dynamics simulation of amyloid-beta (A β 10-35) aggregation. *Molecules*. 2010;15:2730–2748.
- [38] Safarizadeh H, Garkani-Nejad Z. Molecular docking, molecular dynamics simulations and QSAR studies on some of 2-arylethenyl-quinoline derivatives for inhibition of Alzheimer's amyloid-beta aggregation: insight into mechanism of interactions and parameters for design of new inhibitors. *J Mol Graph Model* [Internet]. 2019;87:129–143. DOI:10.1016/j.jmgl.2018.11.019.
- [39] Halder AK, Honarparvar B. Molecular alteration in drug susceptibility against subtype B and C-SA HIV-1 proteases: MD study. *Struct Chem*. 2019;30:1715–1727.
- [40] Ghosh A, Panda P, Halder AK CM. In silico characterization of aryl benzoyl hydrazide derivatives as potential inhibitors of RdRp enzyme of H5N1 influenza virus. *Front Pharmacol* [Internet]. 2022. DOI:10.3389/fphar.2022.1004255
- [41] Srinivasan J, Miller J, Kollman PA, et al. Continuum solvent studies of the stability of rna hairpin loops and helices. *J Biomol Struct Dyn*. 1998;16:671–682.
- [42] Ylilauri M, Pentikäinen OT. MMGBSA as a tool to understand the binding affinities of filamin-peptide interactions. *J Chem Inf Model*. 2013;53:2626–2633.
- [43] La Spada AR. Repeat meeting's repeat performance. *Trends Genet*. 1999;15:350–351.
- [44] Stindt MH, Muller PAJ, Ludwig RL, et al. Functional interplay between MDM2, p63/p73 and mutant p53. *Oncogene*. 2015;34:4300–4310.
- [45] Zhang J, Sun W, Kong X, et al. Mutant p53 antagonizes p63/p73-mediated tumor suppression via Notch1. *Proc Natl Acad Sci U S A*. 2019;116:24259–24267.
- [46] Joerger AC, Bauer MR, Wilcken R, et al. Exploiting transient protein states for the design of small-molecule stabilizers of mutant p53. *Structure* [Internet]. 2015;23:2246–2255. doi:10.1016/j.str.2015.10.016.
- [47] Gomes AS, Ramos H, Gomes S, et al. SLMP53-1 interacts with wild-type and mutant p53 DNA-binding domain and reactivates multiple hotspot mutations. *Biochim Biophys Acta Gen Subj* [Internet]. 2020;1864:129440. DOI:10.1016/j.bbagen.2019.129440.